

Trivariate Spline Collocation Methods for Numerical Solution to 3D Monge-Ampère Equation

Ming-Jun Lai · Jinsil Lee

Received: date / Accepted: date

Abstract We use trivariate spline functions for the numerical solution of the Dirichlet problem of the 3D elliptic Monge-Ampère equation. Mainly we use the spline collocation method introduced in [SIAM J. Numerical Analysis, 2405-2434, 2022] to numerically solve iterative Poisson equations and use an averaged algorithm to ensure the convergence of the iterations. We shall also establish the rate of convergence under a sufficient condition and provide some numerical evidence to show the numerical rates. Then we present many computational results to demonstrate that this approach works very well. In particular, we tested many known convex solutions as well as nonconvex solutions over convex and nonconvex domains and compared them with several existing numerical methods to show the efficiency and effectiveness of our approach.

Keywords Monge-Ampère equation · collocation method · iterative constrained minimization · spline functions

Mathematics Subject Classification (2010) 65N30 · 65K10 · 35J96

1 Introduction

We are interested in numerically solving the Monge-Ampère equation with Dirichlet boundary condition:

$$\det(D^2u(\mathbf{x})) = f(\mathbf{x}), \quad \text{in } \Omega \subset \mathbb{R}^3 \quad (1)$$

$$u(\mathbf{x}) = g(\mathbf{x}), \quad \text{on } \partial\Omega, \quad (2)$$

Ming-Jun Lai, Jinsil Lee
Department of Mathematics, University of Georgia, Athens, GA 30602

Ming-Jun Lai
E-mail: mjlai@uga.edu

Jinsil Lee
E-mail: jl74942@uga.edu

where $\mathbf{x} = (x, y, z)$ has 3 independent variables in a bounded domain $\Omega \subset \mathbb{R}^3$ and D^2u is the Hessian of the function u , more precisely,

$$\det(D^2u) = u_{xx}u_{yy}u_{zz} + 2u_{xy}u_{yz}u_{xz} - u_{xx}(u_{yz})^2 - u_{yy}(u_{xz})^2 - u_{zz}(u_{xy})^2. \quad (3)$$

This is a first step toward to solve the fully nonlinear Monge-Ampère equation

$$\det(D^2u(\mathbf{x})) = f(\mathbf{x})/g(\nabla u(\mathbf{x})), \quad \mathbf{x} \text{ in } \Omega \subset \mathbb{R}^3 \quad (4)$$

$$\nabla u(\mathbf{x})|_{\partial\Omega} = \partial W, \quad (5)$$

where the boundary condition is called the oblique boundary condition. Such a partial differential equation arises from the optimal transportation problem (cf. e.g. [25] and [53]). More specifically, given a density function $f(\mathbf{x})$ on the domain Ω and another density function $g(\mathbf{w})$ on a separate domain W , the goal is to find the optimal plan T which transports f over Ω to g over W under the cost functional $c(\mathbf{x}, \mathbf{w}) = \frac{1}{2}\|\mathbf{x} - \mathbf{w}\|^2$, with $\int_{\Omega} f(\mathbf{x})d\mathbf{x} = \int_W g(\mathbf{w})d\mathbf{w}$. It is Y. Brenier who discovered a characterization of the optimal transportation problem.

Theorem 1 (Brenier, 1988[11]) *Suppose that the transport cost is the quadratic Euclidean distance, $c(x, y) = \frac{1}{2}\|x - y\|^2$ and suppose that W is a convex domain. Then there exists a convex function $u : \Omega \mapsto \mathbb{R}$ satisfying the Monge-Ampère equation (4), unique up to a constant, such that the gradient map $m = \nabla u$ is the unique optimal transport map satisfying the oblique boundary condition $\nabla u|_{\partial\Omega} = \partial W$.*

Although it is hard to determine the oblique boundary condition mentioned above, once we specify a map from the boundary of Ω to the boundary of W , the problem (4) becomes a Neumann boundary problem of the Monge-Ampère equation. In particular, if u is C^2 function whose gradient ∇u transforms Ω onto W , we can move the density $f(\mathbf{x})$ at $\mathbf{x} \in \Omega$ to the location $\nabla u(\mathbf{x}) \in W$ to become the density $g(\nabla u(\mathbf{x}))$. Such a problem is called the free movement problem which will be addressed at the end of this paper.

Instead of considering the Neumann or oblique boundary value problem, this paper will focus on the Monge-Ampère equation with a Dirichlet boundary condition. Note that this PDE has been studied for many years. In addition to the mathematical community, the Monge-Ampère equation has also been broadly studied in many applied fields such as elasticity, geometric optics, and image processing. See [14] and [46]. Today such free-form optics are important in illumination applications. For example, they are used in the automotive industry for the construction of headlights that use the full light emitted by the lamp to illuminate the road but at the same time do not glare oncoming traffic [57]. There are multiple ways to solve this inverse reflector problem; brute-force approaches, methods of supporting ellipsoids, simultaneous multiple surfaces approach, and Monge-Ampère approaches. Also, the Monge-Ampère equation finds applications in finance, seismic wave propagation, geostrophic flows, in differential geometry as explained in [17]. In this paper, we shall explain a spline based collocation method to solve the nonlinear PDE (1).

Let us begin recalling some existence, uniqueness, and regularity property of the Monge-Ampère equation (1). When f, g are sufficiently smooth, the solution of (1) is very smooth explained in the following

Theorem 2 (Theorem 1 in [19]) Suppose that a bounded domain $\Omega \in \mathbb{R}^n$ is strictly convex, where $n \geq 2$. For any strictly positive right-hand side $f \in C^\infty(\bar{\Omega})$ with the boundary condition g which has an extension $g \in C^\infty(\bar{\Omega})$, there exists a unique strictly convex solution u is in $C^\infty(\Omega)$ satisfying (1).

There are several weaker versions of the existence results with regularity properties in the literature. For example,

Theorem 3 (Figalli, 2017 [28]) Let Ω be a uniformly convex domain, $k \geq 2, \alpha \in (0, 1)$, and assume that $\partial\Omega$ is of class $C^{k+2, \alpha}$. Let $f \in C^{k, \alpha}(\bar{\Omega})$ with $f \geq c_0 > 0$. Then for any $g \in C^{k+2, \alpha}(\partial\Omega)$, there exists a unique solution $u \in C^{k+2, \alpha}(\bar{\Omega})$ to the Dirichlet problem (1).

In [4], Awanou introduced another weaker version of the existence theorem:

Theorem 4 (Awanou, 2013[4]) Let Ω be a uniformly convex domain in \mathbb{R}^n with boundary in C^3 . Suppose $g \in C^3(\bar{\Omega})$, $\inf f > 0$, and $f \in C^\alpha(\bar{\Omega})$ for some $\alpha \in (0, 1)$. Then (1) has a convex solution u which satisfies the a priori estimate

$$\|u\|_{C^{2, \alpha}(\bar{\Omega})} \leq C,$$

where C depends only on $n \geq 2, \alpha, \inf f, \Omega, \|f\|_{C^\alpha(\bar{\Omega})}$ and $\|g\|_{C^3}$.

In general, there are at least three different notions of solutions which have been studied in the literature besides the classic solution: one is called Aleksandrov solution, another one is viscosity solution, and the next one is Brainer's solution, according to the monograph by Villani, 2003, see page 129 in [53]. The theory for the Monge-Ampère equation is deep (cf. [20], [25], [53] and [54]). In particular, the regularity of the solution has been extensively studied (cf. e.g. [18], [55], [22]). In a landmark paper [18], Caffarelli showed that the solution of the Monge-Ampère equation has an interior regularity over $\Omega' \subset \Omega$, i.e. $u \in H^{2, p}(\Omega')$ for any open set Ω' inside Ω . Furthermore, the solution has H^2 regularity over the entire domain, as established in [55]:

Theorem 5 (Wang, 1996[55]) Let Ω be a strictly convex domain in \mathbb{R}^n . If $\partial\Omega$ and g in the equation (2) are C^3 smooth, and $f(x) \in C^{1,1}(\bar{\Omega})$, then the solution $u \in C^{2+\alpha}(\bar{\Omega})$.

Due to these regularity results, we can use C^2 smooth trivariate splines to approximate the solution u under the conditions $f \in C^{1,1}(\bar{\Omega})$, $g \in C^3(\partial\Omega)$ and Ω being a strictly convex domain. In our computation, we are able to solve the Monge-Ampère equation over domains with uniform positive reach (cf. [31]) which include strictly convex domains as a special case. Additionally, we can use our method to experiment with the solution (1) even when f is not in $C^{1,1}(\bar{\Omega})$.

The numerical solution of the Monge-Ampère equation (MAE) is an active area of research, with many researchers developing different numerical methods and analyzing their theoretical convergence. As mentioned in [12], the MAE poses several challenges for numerical solutions. The first challenge is that the equation is fully nonlinear, which means that geometric solutions or viscosity solutions must be used as weak solutions. The second challenge is the convex constraint, as the equation might not have a unique solution without it.

The popular finite element method is not directly applicable because of the involvement of the Hessian of the solution. This restricts the use of the Finite Element Method (FEM) or general Galerkin projection methods, discontinuous Galerkin method or continuous Galerkin method. However, there are several remedy approaches based on the finite element method such as a mixed finite element method, vanishing moment method, etc. See [3], [5], [9] and [27].

Besides of finite element type methods, there are many finite difference methods, as seen in [12], [7], [44], [13], [43]. Moreover, many interesting approaches are based on the classic finite difference method as demonstrated in [15], [45], [13]. However, these methods have a weakness: they do not have analytic form of solution over the entire domain. In addition, we can find time marching methods in [6], [4], and least squares relaxation methods in [23], [24], [17].

Let us be more precise on the numerical methods mentioned above. The least square notion of the solution was proposed and studied in [23], [24], and [17]. Especially, this least square approach using a relaxation algorithm of the Gauss-Seidel-type iterations to decouple differential operators in [17]. The approximation relies on mixed low order finite element methods with regularization techniques. Several 3D examples were demonstrated to show the performance of this method. In this paper, we will compare the numerical results from our method to those to in [17] to show that our method produces more accurate results. These comparisons will be presented in the last section.

In [6], a time marching approach is used to solve the Monge-Ampère equation . Given $\nu > 0$, the researcher considered the sequence of iterates

$$-\nu \Delta u_{k+1} = -\nu \Delta u_k + \det D^2 u_k - f, \quad u_{k+1} = g \quad \text{on } \partial\Omega. \quad (6)$$

He used the discrete version of Newton's method in the vanishing moment methodology. And he showed the convergence of the iterative method for solving the nonlinear system. We shall also compare his numerical results with our results in the last section to show that our proposed method is also more accurate.

In [13], the researchers introduced the meshless Generalized Finite Difference Method (GFDM) in both 2D and 3D settings. They tested several examples using the Cascadic iterative algorithm over convex and non-convex domains. We will compare our proposed method with the results from the Cascadic iterative algorithm in the last section to demonstrate that our method is also better.

We now describe our numerical method to solve (1) by using trivariate spline functions over a tetrahedralization of Ω . See [40], [8], [51], [39] for theoretical properties and numerical implementation of bivariate/trivariate spline functions. In addition, there are several dissertations written to explain how to implement and how to use multivariate splines for the numerical solution of Helmholtz equations, Maxwell equations and 3D surface reconstruction. See [2], [47] and [56]. There are several reasons why we use trivariate splines for the numerical solution of the Monge-Ampère equation . One is that we can use trivariate splines with smoothness $r \geq 2$ to approximate the solution u of the Monge-Ampère equation over an arbitrary convex polyhedral domain. Due to the C^2 smoothness of spline function, we can calculate the Hessian of the solution, so that we simply use the collocation method instead of the

weak formulations in [3], [5], etc.. Many researchers adopted the iterative algorithm called the fixed point algorithm introduced in [12]:

$$\Delta u_{k+1} = ((\Delta u_k)^n + a(f - \det D^2 u_k))^{\frac{1}{n}} \quad (7)$$

along with the prescribed Dirichlet boundary conditions with $a = 2$ and $n = 2$. The researchers in [12] explained that this is a fixed point method as the true solution u satisfies (7) trivially.

In [6], this iterative algorithm is generalized to the 3D setting with $n \geq 3$ for various $a > 0$. In particular, the researcher in [6] explained that the iteration (7) is well-defined for $a \leq n^n$ as $\det(D^2 u_k) \leq \frac{1}{n^2}(\Delta u)^n$. Numerical results in [6] are demonstrated in the framework of the spline element method with $a = 2$ for the 2D case and $a = 9$ for the 3D case.

In this paper, we shall use the following iterative method:

$$\Delta u_{k+1} = ((\Delta u_k)^n + n^n(f - \det D^2 u_k))^{\frac{1}{n}} \quad (8)$$

to handle the nonlinearity of the Monge-Ampère equation where $n = 3$.

However, another requirement of the solution of the Monge-Ampère equation is that u must be convex in order for the equation to be elliptic. Without this constraint, the equation does not have a unique solution. (For example, taking boundary data $g = 0$, if u is a solution, then $-u$ is also a solution in \mathbb{R}^2 .) Many numerical methods mentioned above failed to enforce this convexity constraint. The convexity of u is equivalent to the positive definiteness of the Hessian matrix $D^2 u$. In terms of the eigenvalues $\lambda_1 \geq \lambda_2 \geq \lambda_3$ of $D^2 u$, we will ensure that three eigenvalues $\lambda_1(k) \geq \lambda_2(k) \geq \lambda_3(k)$ of the k th iteration u_k in a spline space satisfy $\lambda_1(k) + \lambda_2(k) + \lambda_3(k) \geq 0$ as well as $\lambda_1(k)\lambda_2(k)\lambda_3(k) > 0$, although they are not enough to ensure the convexity of k th spline solution u_k .

This paper is organized as follows. In Section 2, we first explain trivariate splines, domains with uniformly positive reach, and the spline collocation method for the Poisson equation which is the same as the one discussed in [39]. In Section 3, we introduce the spline collocation method for the Monge-Ampère equation and its average algorithm, and establish three different versions of convergence results. Finally, in the last section 4, we present numerical results for several 3D examples of smooth and convex solutions, as well as nonsmooth convex solution over convex and nonconvex bounded domains to demonstrate the effectiveness of our proposed method. We compare our results with those of several existing numerical methods to show the accuracy and efficiency of our method. Finally, we shall present some examples for the free movement in 2D and 3D settings to show how the density from one place is moved to another place. This will demonstrate further that our proposed method is versatile enough.

2 Preliminaries

2.1 Trivariate Splines

Let us quickly summarize the essentials of trivariate splines in this section. Given a tetrahedron T , we write $|T|$ for the length of its longest edge, and ρ_T for the radius of the largest inscribed ball in T . For any polygonal domain $\Omega \subset \mathbb{R}^3$, let $\Delta := \{T_1, \dots, T_n\}$ be a tetrahedralization of Ω which is a collection of tetrahedra and \mathcal{V} be the set of vertices of Δ . We called a tetrahedralization as a quasi-uniform tetrahedralization if all tetrahedra T in Δ have comparable sizes in the sense that

$$\frac{|T|}{\rho_T} \leq C < \infty, \quad \text{all tetrahedra } T \in \Delta,$$

where ρ_T is the inradius of T . Let $|\Delta|$ be the length of the longest edge in Δ .

Next for a tetrahedron $T = (\mathbf{v}_1, \mathbf{v}_2, \mathbf{v}_3, \mathbf{v}_4) \in \Delta$, we define the barycentric coordinates (b_1, b_2, b_3, b_4) of a point $(x, y, z) \in \Omega$ as the solution to the following system of equations

$$\begin{aligned} b_1 + b_2 + b_3 + b_4 &= 1 \\ b_1 v_{1,x} + b_2 v_{2,x} + b_3 v_{3,x} + b_4 v_{4,x} &= x \\ b_1 v_{1,y} + b_2 v_{2,y} + b_3 v_{3,y} + b_4 v_{4,y} &= y \\ b_1 v_{1,z} + b_2 v_{2,z} + b_3 v_{3,z} + b_4 v_{4,z} &= z, \end{aligned}$$

where the vertices $\mathbf{v}_i = (v_{i,x}, v_{i,y}, v_{i,z})$ for $i = 1, 2, 3, 4$. b_1, \dots, b_4 are nonnegative if $(x, y, z) \in T$. Next we use the barycentric coordinates to define the Bernstein polynomials of degree D :

$$B_{i,j,k,\ell}^T(x, y, z) := \frac{D!}{i!j!k!\ell!} b_1^i b_2^j b_3^k b_4^\ell, \quad i + j + k + \ell = D,$$

which form a basis for the space \mathcal{P}_D of polynomials of total degree D . Therefore, we can represent all $s \in \mathcal{P}_D$ in B-form:

$$s|_T = \sum_{i+j+k+\ell=D} c_{ijk\ell}^T B_{ijk\ell}^T, \quad \forall T \in \Delta,$$

where the B-coefficients $c_{i,j,k,\ell}^T$ are uniquely determined by s . Let $\mathbf{c} = \{c_{ijk\ell}^T, i + j + k + \ell = D, T \in \Delta\}$ be the coefficient vector associated with spline function s .

Moreover, for given $T = (\mathbf{v}_1, \mathbf{v}_2, \mathbf{v}_3, \mathbf{v}_4) \in \Delta$, we define the associated set of domain points to be

$$\mathcal{D}_{D,T} := \left\{ \frac{i\mathbf{v}_1 + j\mathbf{v}_2 + k\mathbf{v}_3 + \ell\mathbf{v}_4}{D} \right\}_{i+j+k+\ell=D}. \quad (9)$$

Let $\mathcal{D}_{D,\Delta} = \cup_{T \in \Delta} \mathcal{D}_{D,T}$ be the domain points of tetrahedral Δ and degree D .

We use the discontinuous spline space $S_D^{-1}(\Delta) := \{s|_T \in \mathcal{P}_D, T \in \Delta\}$ as a base. Then we add the smoothness conditions to define the space $S_D^r := C^r(\Omega) \cap S_D^{-1}(\Delta)$. The smoothness conditions are explained in [40]. Indeed, see Theorem 15.31 in [40].

We use C^r smooth spline functions in $H^2(\Omega)$ with $r \geq 1$ and the degree D of splines sufficiently large satisfying $D \geq 3r + 2$ in \mathbb{R}^2 and $D \geq 6r + 3$ in \mathbb{R}^3 . And we get the following Lemma in [40]

Lemma 1 *For all $u \in W^{m+1,p}(\Omega)$ for some $0 \leq m \leq D$ and $1 \leq p \leq \infty$, there exists a quasi-interpolatory spline $s_u \in \mathcal{S}_D^r(\Delta)$ such that*

$$\|D^\alpha(u - s_u)\|_{L^p(\Omega)} \leq C|\Delta|^{m+1-|\alpha|}|u|_{m+1,p,\Omega},$$

for all $0 \leq |\alpha| \leq m$, where $|\cdot|_{m+1,p,\Omega}$ is a semi-norm, C is a positive constant independent of u and $|\Delta|$ but is dependent on the geometry of Δ .

In addition, we shall use Markov inequality(cf. [40]):

$$\|\nabla s\|_{\infty,\Omega} \leq \frac{C}{|\Delta|} \|s\|_{\infty,\Omega}, \quad \forall s \in \mathcal{S}_D^r(\Delta) \quad (10)$$

for a positive constant C independent of s and the size $|\Delta|$ of tetrahedralization Δ .

2.2 Domains with Uniformly Positive Reach

Let us recall a concept on domains of interest explained in [31].

Definition 1 Let $K \subseteq \mathbb{R}^n$ be a non-empty set. Let r_K be the supremum of the number r such that every points in

$$P = \{x \in \mathbb{R}^n : \text{dist}(x, K) < r\}$$

has a unique projection in K . The set K is said to have a positive reach if $r_K > 0$.

A domain with C^2 boundary has a positive reach. Sets of positive reach are much more general than convex sets. Let $B(0, \epsilon)$ be the closed ball centering at 0 with radius $\epsilon > 0$, and let K^c stand for the complement of the set $K \in \mathbb{R}^n$. For any $\epsilon > 0$, the set

$$E_\epsilon(K) := (K^c + B(0, \epsilon))^c \subseteq K$$

is called an ϵ -erosion of K . Next we recall the following definition from [31].

Definition 2 A set $K \subseteq \mathbb{R}^n$ is said to have a uniformly positive reach r_0 if there exists some $\epsilon_0 > 0$ such that for all $\epsilon \in [0, \epsilon_0]$, $E_\epsilon(K)$ has a positive reach at least r_0 .

Many examples of domains with positive reach can be found in [31]. And we have the following property about these domains

Lemma 2 *If $\Omega \subset \mathbb{R}^n$ is of positive reach r_0 , then for any $0 < \epsilon < r_0$, the boundary of $\Omega_\epsilon := \Omega + B(0, \epsilon)$ containing Ω is of $C^{1,1}$. Furthermore, Ω_ϵ has a positive reach $\geq r_0 - \epsilon$.*

In [31], Gao and Lai proved the following regularity theorem

Theorem 6 *Let Ω be a bounded domain. Suppose the closure of Ω is of uniformly positive reach r_Ω . For any $f \in L^2(\Omega)$, let $u \in H_0^1(\Omega)$ be the unique weak solution of the Dirichlet problem:*

$$\begin{cases} -\Delta u &= f \text{ in } \Omega \\ u &= 0 \text{ on } \partial\Omega \end{cases}$$

Then $u \in H^2(\Omega)$ in the sense that

$$\sum_{i,j=1}^n \int_{\Omega} \left(\frac{\partial^2 u}{\partial x_i \partial x_j} \right)^2 \leq C_0 \int_{\Omega} f^2 dx$$

for a positive constant C_0 depending only on r_Ω .

2.3 A Collocation Method for the Poisson Equation

For convenience, let us start with the Poisson equation

$$\begin{aligned} \Delta u(\mathbf{x}) &= f(\mathbf{x}) \quad \forall \mathbf{x} \in \Omega \subset \mathbb{R}^3 \\ u(\mathbf{x}) &= g(\mathbf{x}), \quad \forall \mathbf{x} \in \partial\Omega \end{aligned} \quad (11)$$

For given Δ , let it be a tetrahedral partition of Ω , we choose a set of domain points $\{\xi_i\}_{i=1,\dots,N}$ explained in the previous section as collocation points and let $s = \sum_{t \in \Delta} \sum_{|\alpha|=D} c_\alpha^t \mathcal{B}_\alpha^t$ in $\mathcal{S}_D^r(\Delta)$ with the coefficient vector \mathbf{c} of s . Then we want to find the coefficient vector \mathbf{c} of spline function satisfying the standard Poisson equation (11) at those collocation points

$$\begin{cases} \Delta s(\xi_i) &= f(\xi_i), \quad \xi_i \in \Omega \subset \mathbb{R}^n, \\ s(\xi_i) &= g(\xi_i), \quad \xi_i \in \partial\Omega, \end{cases} \quad (12)$$

where $\{\xi_i\}_{i=1,\dots,N} \in \mathcal{D}_{D',\Delta}$ are the domain points of Δ of degree $D' > 0$ as explained in (9) in the previous section, where D' will be different from D ($D' > D$).

Using these points, we let K be the following matrix:

$$K := \left[\Delta(B_{i,j,k,l}^t)(\xi_i) \right].$$

In general, the spline s with coefficients in \mathbf{c} is a discontinuous function. In order to make $s \in \mathcal{S}_D^r(\Delta)$, its coefficient vector \mathbf{c} must satisfy the constraints $H\mathbf{c} = 0$ for the smoothness conditions that the $\mathcal{S}_D^r(\Delta)$ functions possess (cf. [40]). Based on the smoothness conditions (cf. Theorem 2.28 or Theorem 15.38 in [40]), we can construct matrices H for the C^r smoothness conditions. Then, our collocation method is to find \mathbf{c} which solves the following constrained minimizations:

$$\min_{\mathbf{c}} J(\mathbf{c}) = \frac{1}{2} (\|B\mathbf{c} - G\|^2 + \|H\mathbf{c}\|^2) \quad (13)$$

$$\text{subject to } K\mathbf{c} = \mathbf{f} \quad (14)$$

where B, G are from the boundary condition and H is from the smoothness condition. Note that we need to justify that the minimization has a solution. In general, we do not know if $K\mathbf{c} = \mathbf{f}$ has a solution or not. However, we can show that a neighborhood of $K\mathbf{c} = \mathbf{f}$, i.e.

$$\mathbb{N} = \{\mathbf{c} : \|K\mathbf{c} - \mathbf{f}\| \leq \epsilon\} \quad (15)$$

is not empty for an appropriate $\epsilon > 0$ when $|\Delta|$ is small enough. Indeed, let us use spline approximation theorem (cf. [40]) to have

Lemma 3 *Suppose that Ω is a polygonal domain. Suppose that $u \in H^3(\Omega)$. Then there exists a spline function $u_s \in S_D^r(\Delta)$ and a positive constant \hat{C} depending on $D \geq 1$ and $D' > D$ such that*

$$\|\Delta u(x, y, z) - \Delta u_s(x, y, z)\|_{L^\infty(\Omega)} \leq \epsilon_1 \hat{C}$$

where ϵ_1 is a given tolerance and \hat{C} depends on Ω, D, D' .

We thus consider a nearby problem of the minimization (13), which is:

$$\min_{\mathbf{c}} \|B\mathbf{c} - G\|^2 + \|H\mathbf{c}\|^2, \quad (16)$$

$$\text{subject to } \|K\mathbf{c} - \mathbf{f}\|_{L^\infty} \leq \epsilon_1. \quad (17)$$

It is easy to see that the minimizer of (16) clearly approximates the minimizer of (13) if $\epsilon_1 \ll 1$. As the new minimization problem is convex and the feasible set is also convex, the minimization (16) will have a unique solution if the feasible set is non-empty.

We may assume that our numerical solution u_s approximates u on $\partial\Omega$ very well in the sense that $\|u - u_s\| \leq C\epsilon_2$ for a positive constant C . Denote $\|u\|_L := \|\Delta u\|_{L^2(\Omega)}$. In [39], Lai and Lee proved the following theorems

Theorem 7 *Suppose f and g are continuous over bounded domain $\Omega \subseteq \mathbb{R}^d$ for $d = 2$ or $d = 3$. Suppose that $u \in H^3(\Omega)$. When Ω is a domain with uniform positive reach, we have the following inequality*

$$\|u - u_s\|_{L^2(\Omega)} \leq C\|u - u_s\|_L, \quad \|\nabla(u - u_s)\|_{L^2(\Omega)} \leq C\|u - u_s\|_L$$

and

$$\sum_{i+j=2} \left\| \frac{\partial^2}{\partial x^i \partial y^j} u \right\|_{L^2(\Omega)} \leq C\|u - u_s\|_L$$

for a positive constant C depending on Ω .

And we can obtain the better convergence results if we assume that $|u - u_s|_{\partial\Omega} = 0$, as shown in the following theorem:

Theorem 8 *Suppose that $|u - u_s|_{\partial\Omega} = 0$. Under the assumptions in Theorem 7, we have the following inequality*

$$\|u - u_s\|_{L^2(\Omega)} \leq C|\Delta|^2(\|u - u_s\|_L) \text{ and } \|\nabla(u - u_s)\|_{L^2(\Omega)} \leq C|\Delta|(\|u - u_s\|_L)$$

for a positive constant C , where $|\Delta|$ is the size of the underlying tetrahedral Δ .

Proof We use the same arguments as in [39] to establish a proof.

3 Our Proposed Algorithms and Their Convergence Analysis

3.1 A Spline Based Collocation Method for Monge-Ampère Equation

For convenience, let us explain our spline based collocation method for the 3D Monge-Ampère equation first. In the 3D setting, we will solve the following iterative equations as in [6]

$$\Delta u_{k+1} = \sqrt[3]{(\Delta u_k)^3 + a(f - \det(D^2 u_k))}, \quad k = 0, 1, \dots, \quad (18)$$

with an initial u_0 by solving

$$\Delta u_0 = \sqrt[3]{27f}$$

together with the given boundary condition. Let us make two quick remarks. The initial u_0 so chosen is based on the following assumption. Writing $\lambda_i, i = 1, 2, 3$, to be the eigenvalues of $\det(D^2 u)$, the Monge-Ampère equation reads $\lambda_1 \lambda_2 \lambda_3 = f$. If these eigenvalues are close to each other, e.g. all are equal to λ , we have $\lambda^3 = f$ and thus $\lambda = \sqrt[3]{f}$. Since $\Delta u = \lambda_1 + \lambda_2 + \lambda_3$, we get $\Delta u = 3\lambda = 3\sqrt[3]{f} = \sqrt[3]{27f}$. However, when these eigenvalues are quite different, such a choice of initial u_0 may not be a good one. We shall explain our approach later in this section.

Next about the parameter a in (18), we have tested different numbers for a . Figure 1 shows that we can get more accurate results when using $a = 27$. We will use $a = 27$ in the rest of the paper.

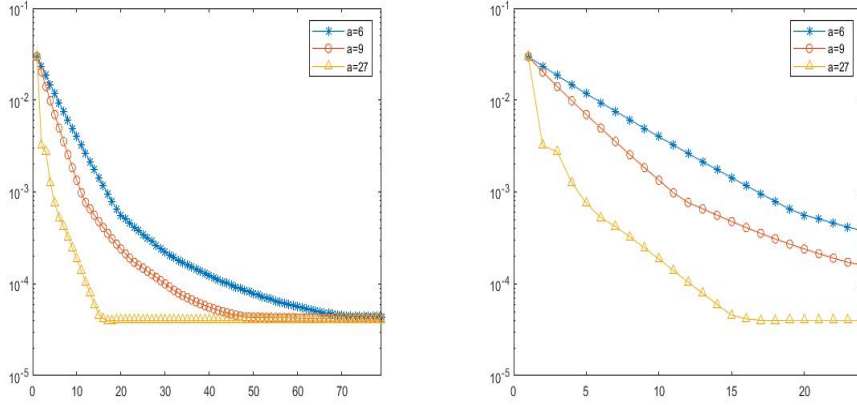


Fig. 1 $\log(\|u - u_s^{(k)}\|_\infty)$ (y-axis) for u^{3d3} (left) and u^{3d5} (right) for each iteration(x-axis) with different $a = 6, 9, 27$

For simplicity, we use the Dirichlet boundary condition $u|_{\partial\Omega} = g$ to explain our numerical method.

3.2 Two Computational Algorithms

We shall present two computational algorithms for numerical solution of the Monge-Ampère equation. The first one is a standard approach which has been used by many researchers based on finite different discretization and finite element discretization in the literature. We shall use multivariate spline functions to discretize the function space $H^2(\Omega)$ to demonstrate the efficiency and effectiveness of our multivariate spline approach as well as show that our numerical results are better than many methods in the literature. See our computational results in the next section.

Algorithm 1: An Iterative Poisson Equation Algorithm

Start with an initial solution u_0 by solving the following Poisson equation using our collocation method discussed in the previous section:

$$\Delta u_0 = \sqrt[3]{27f} \quad (19)$$

and $u_0 = g$ on the boundary $\partial\Omega$. We then iteratively solve the Poisson equation

$$\Delta u_{k+1} = \sqrt[3]{(\Delta u_k)^3 + 27(f - \det(D^2 u_k))}, \quad k = 0, 1, \dots \quad (20)$$

That is, we find $u_{k+1} \in S_D^r(\Delta)$ satisfying the following equations approximately:

$$\begin{cases} \Delta u_{k+1}(\xi_i) = \sqrt[3]{(\Delta u_k(\xi_i))^3 + 27(f(\xi_i) - \det(D^2 u_k(\xi_i)))} & \xi_i \in \Omega \subset \mathbb{R}^3, \\ u_{k+1}(\xi_i) = g(\xi_i), & \xi_i \in \partial\Omega \end{cases} \quad (21)$$

In other words, we numerically solve (16) with

$$\mathbf{f}_k = \sqrt[3]{(\Delta u_k(\xi_i))^3 + 27(f(\xi_i) - \det(D^2 u_k(\xi_i)))}$$

by using the iterative algorithm in [39].

Terminate the iteration when $\|f - \det(D^2 u_{k+1})\|_{L^\infty} > \|f - \det(D^2 u_k)\|_{L^\infty}$.

Next we explain an averaged iterative algorithm. Assume Ω is bounded and the closure of Ω is of uniformly positive reach as explained in the previous section. For any $f \in L^2(\Omega)$, the solution of the Poisson equation with zero boundary condition is in $H^2(\Omega)$ by Theorem 6. Furthermore, the solution of the Poisson equation with boundary condition g is in $H^2(\Omega)$ if $g \in H^{1/2}(\partial\Omega)$. Indeed, we consider a function $v \in H^2(\Omega)$ whose trace on $\partial\Omega$ is $g \in H^{1/2}(\partial\Omega)$. Define $w = u - v$ and we have

$$\begin{aligned} \int_{\Omega} \nabla w \cdot \nabla \phi &= \int_{\Omega} \nabla u \cdot \nabla \phi - \int_{\Omega} \nabla v \cdot \nabla \phi \\ &= \int_{\Omega} -f \cdot \phi - \int_{\Omega} \Delta v \cdot \phi = \int_{\Omega} (\Delta v - f) \cdot \phi. \end{aligned}$$

for every $\phi \in H_0^1(\Omega)$. Then the solution w satisfying the weak formulation of

$$\Delta w = f - \Delta v \text{ in } \Omega, w = 0 \text{ on } \partial\Omega$$

is in $H^2(\Omega)$ (cf. [31]). Therefore, $u = w + v$ is in $H^2(\Omega)$.

Let T be an operator which maps $H^2(\Omega) \rightarrow H^2(\Omega)$ in the following sense: for any $v \in H^2(\Omega)$, let $u = T(v)$ be the solution of the Poisson equation:

$$\Delta u = \sqrt[3]{(\Delta v)^3 + 27(f - \det(D^2 v))} \text{ over } \Omega$$

and $u|_{\partial\Omega} = g$ with $g \in H^{1/2}(\partial\Omega)$. In other words, the operator T on $H^2(\Omega)$ is defined by

$$T(u) = \Delta^{-1}[\sqrt[3]{(\Delta u)^3 + 27(f - \det(D^2 u))}].$$

It is easy to see that T is a nonlinear operator T maps $H^2(\Omega)$ to $H^2(\Omega)$. Also, we can see that the exact solution u^* satisfying $\det(D^2 u^*) = f$ is a fixed point of T .

Now we are ready to define an averaged iterative algorithm. In this way, we can find more accurate solutions than the one using Algorithm 1 only.

Algorithm 2: The Averaged Iterative Algorithm

Start with an initial u_0 , where $\Delta u_0 = \sqrt[3]{27f}$ over Ω and $u_0 = g$ on $\partial\Omega$.
We iteratively solve the Poisson equations

$$\Delta u_{k+\frac{1}{2}} = \sqrt[3]{(\Delta u_k)^3 + 27(f - \det(D^2 u_k))}, \quad (22)$$

together with the boundary condition $u_{k+\frac{1}{2}} = g$ on $\partial\Omega$ by using the minimization in (16) and then take

$$u_{k+1} = \frac{1}{2}u_{k+\frac{1}{2}} + \frac{1}{2}u_k. \quad (23)$$

Stop the iteration if $\|f - \det(D^2 u_{k+1})\|_{L^\infty} > \|f - \det(D^2 u_k)\|_{L^\infty}$.

Let us present some performance of these two algorithms to show that Algorithm 2 indeed very useful. Consider a testing function u^{3ds1} as in Section 4, the eigenvalues of the Hessian matrix $D^2 u^{3ds1}$ are 1, 5, 15. Although these three eigenvalues are not close to any real positive number, we use various positive numbers p for the right-hand side of the Poisson equation $\Delta u_0 = p$ to solve u_0 as an initial solution and then apply Algorithm 1 and Algorithm 2. In Table 1, the results from both Algorithms are shown after the same number of iterations. We can see that Algorithm 2 produces more accurate solution than Algorithm 1 from various initial values except for p which is close to $21 = \Delta u^{3ds1}$, i.e. $p \in [17.7, 26]$. Also, the ℓ_2 and h_1 errors from Algorithm 2 are better than the errors from Algorithm 1 for testing functions u^{3ds3} and u^{3ds8} as shown in Figure 2.

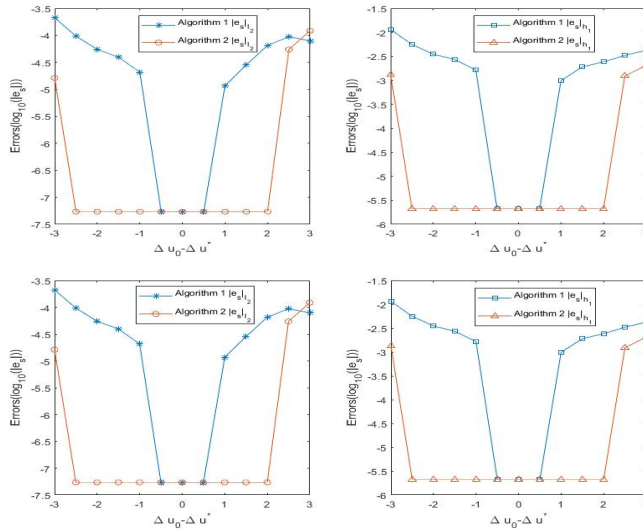
3.3 Convergence Analysis

According to [5], it is known that if $\det(D^2 u^*) = f > 0$ and u^* is convex, then there exist constants $m, M > 0$, independent of the mesh size $|\Delta|$ such that

$$0 < m \leq \lambda_3 \leq \lambda_2 \leq \lambda_1 \leq M,$$

Table 1 Errors of numerical solutions u^{3ds1} for the Monge Ampère equation over $[0, 1]^3$ with $D = 9$, $r = 1$ over the same tetrahedralization for various initial values p by two algorithms

$\Delta u_0 = p$	Algorithm 1		Algorithm 2	
	$ e_s _{l_2}$	$ e_s _{h_1}$	$ e_s _{l_2}$	$ e_s _{h_1}$
12.6	2.1291e-02	1.6315e-01	1.9230e-02	1.3670e-01
15.1	3.4135e-03	5.8902e-02	5.0004e-03	5.1503e-02
16.4	2.0124e-03	3.1978e-02	1.2081e-08	5.4356e-07
17.1	7.9130e-04	1.4517e-02	4.1401e-08	1.6448e-06
17.7	1.3980e-09	3.9929e-08	3.6103e-08	2.7446e-06
26.0	6.4074e-09	2.4003e-07	4.8324e-07	1.8097e-05
26.5	2.0899e-04	6.3176e-03	5.0149e-07	1.8781e-05
27.0	5.6423e-04	1.7172e-02	3.9592e-04	1.2049e-02
27.5	8.9037e-04	2.5381e-02	7.0701e-04	2.0696e-02

**Fig. 2** Errors $\log(|e_s|_{l_2})$, $\log(|e_s|_{h_1})$ for u^{3ds3} (Top) and u^{3ds8} (Bottom)

where $\lambda_1, \lambda_2, \lambda_3$ are the eigenvalues of $(D^2u(x))$, $\forall x \in \Omega$. The following result is also known (cf. [6]). For clarity, we provide a proof below.

Lemma 4 Suppose that the convex solution $u^* \in W^{2,\infty}$ satisfies $\det(D^2u^*) = f > 0$. There exists a $\delta > 0$ such that for any u which is close enough to the exact solution u^* in the sense that $|u - u^*|_{2,\infty} \leq \delta$, we have

$$\det(D^2u) \leq \frac{1}{27}(\Delta u)^3 < \frac{1}{a}(\Delta u)^3$$

for any $a < 27$.

Proof Recall that the eigenvalues of a symmetric matrix are continuous functions of its entries, as roots of the characteristic equation (cf. Ostrowski (1960) Appendix K [49]). Thus, for a given $u^* \in W^{2,\infty}(\Omega)$, there exists $\delta > 0$ such that for $u \in W^{2,\infty}(\Omega)$, $|u -$

$u^*|_{2,\infty} \leq \delta$ implies $M \geq \lambda_1(D^2u(x)) \geq \lambda_2(D^2u(x)) \geq \lambda_3(D^2u(x)) > 0$. Now, we use the property that $\det(D^2u)$ is the multiplication of all eigenvalues to have

$$\begin{aligned} \det(D^2u) &= \lambda_1\lambda_2\lambda_3 = \frac{1}{27}(3\lambda_1\lambda_2\lambda_3 + 6\lambda_1\lambda_2\lambda_3 + 18\lambda_1\lambda_2\lambda_3) \\ &\leq \frac{1}{27}(\lambda_1^3 + \lambda_2^3 + \lambda_3^3 + 6\lambda_1\lambda_2\lambda_3 + 3\lambda_3(\lambda_1^2 + \lambda_2^2) + 3\lambda_1(\lambda_2^2 + \lambda_3^2) + 3\lambda_2(\lambda_1^2 + \lambda_3^2)) \\ &= \frac{1}{27}(\lambda_1 + \lambda_2 + \lambda_3)^3 = \frac{1}{27}(\Delta u)^3. \end{aligned}$$

This completes all the proof. \square

We first consider the point-wise convergence of the sequence from Algorithm 1.

Theorem 9 Fix a spline space $\mathcal{S}_D^r(\Delta)$ with Δ being a tetrahedralization of the domain Ω . Let $u_k \in \mathcal{S}_D^r(\Delta)$, $k \geq 1$ be the sequence from Algorithm 1. Then, any average values of $f - \det(D^2u_k)$, $k \geq 1$ are nonnegative in the following senses:

$$\frac{1}{n+1} \sum_{k=0}^n (f(\mathbf{x}) - \det(D^2u_k)(\mathbf{x})) \geq 0, \quad \mathbf{x} \in \Omega \quad (24)$$

for all $n \geq 1$. Furthermore, suppose that there exists a bound $M > 0$ such that $|u_k(\mathbf{x})| \leq M$ over Ω for all $k \geq 0$. Then

$$\frac{1}{n+1} \sum_{k=0}^n (f(\mathbf{x}) - \det(D^2u_k)(\mathbf{x})) \rightarrow 0 \quad (25)$$

when $n \rightarrow \infty$ for all $\mathbf{x} \in \Omega$.

We remark that the condition that $|u_k(\mathbf{x})| \leq M$ above is a computational condition one can check during the iterative computation of Algorithm 1. Our numerical experiments show that for some testing functions u , this condition does satisfy while for other testing functions, the condition does not satisfy. See Figure 3 for these numerical phenomena.

Proof By (21) and Lemma 4, we get

$$\begin{aligned} 27\det(D^2u_{k+1}) &\leq (\Delta u_{k+1})^3 = (\Delta u_k)^3 + 27(f - \det(D^2u_k)) \\ &= (\Delta u_{k-1})^3 + 27(f - \det(D^2u_{k-1})) + 27(f - \det(D^2u_k)) \\ &= (\Delta u_{k-1})^3 + 2 \cdot 27f - 27\det(D^2u_{k-1}) - 27\det(D^2u_k) \\ &= \dots \\ &= (\Delta u_0)^3 + 27(k+1)f - 27 \sum_{j=0}^k \det(D^2u_j) \\ &= 27f + 27(k+1)f - 27 \sum_{j=0}^k \det(D^2u_j). \end{aligned}$$

Hence, we have

$$0 \leq 27f + 27(k+1)f - 27 \sum_{j=0}^k \det(D^2 u_j) - 27 \det(D^2 u_{k+1}) = 27 \sum_{j=0}^{k+1} (f - \det(D^2 u_j)).$$

which leads to (24). In addition, we also have

$$(\Delta u_{k+1})^3 - (\Delta u_0)^3 = 27 \sum_{j=0}^k (f - \det(D^2 u_j)).$$

By the assumption of this theorem, u_{k+1} has a bound, i.e. $\|u_{k+1}\|_{\infty, \Omega} \leq M$. Then we can use the Markov inequality to have

$$\|\Delta u_{k+1}\|_{\infty, \Omega} \leq \frac{C}{|\Delta|^2} \|u_{k+1}\|_{\infty, \Omega} \leq \frac{CM}{|\Delta|^2} < \infty \quad (26)$$

for a constant $C > 0$ independent of u_{k+1} . It thus follows

$$\frac{27 \sum_{j=0}^k (f - \det(D^2 u_j))}{k+1} = \frac{(\Delta u_{k+1})^3 - (\Delta u_0)^3}{k+1} \rightarrow 0.$$

Therefore, we finished a proof of Theorem 9. \square

Furthermore, we denote $w(u, f) := \sqrt[3]{(\Delta u)^3 + 27(f - \det(D^2 u))}$. We have

$$\begin{aligned} \|\Delta u_{k+1} - \Delta u\|_{L^2(\Omega)} &= \left\| \frac{(\Delta u_k)^3 + 27(f - \det(D^2 u_k)) - (\Delta u)^3}{(w(u_k, f))^2 + w(u_k, f)w(u, f) + (w(u, f))^2} \right\|_{L^2(\Omega)} \\ &= \left\| \frac{(\Delta u_k)^3 - (\Delta u)^3 + 27(\det(D^2 u) - \det(D^2 u_k))}{(w(u_k, f))^2 + w(u_k, f)w(u, f) + (w(u, f))^2} \right\|_{L^2(\Omega)} \end{aligned}$$

By simple calculations, we get

$$(\Delta u_k)^3 - (\Delta u)^3 = (\Delta u_k - \Delta u)((\Delta u_k)^2 + \Delta u_k \cdot \Delta u + (\Delta u)^2)$$

and by Lemmas 2.1, 2.2 and 2.3 in [5]

$$\det(D^2 u) - \det(D^2 u_k) = \text{cof}((1-t)D^2 u_k + tD^2 u) : (D^2 u_k - D^2 u)$$

for some $t \in [0, 1]$. By simple calculation and Lemma 5, we have

$$\begin{aligned} &\left\| \frac{(\Delta u_k)^3 - (\Delta u)^3}{(w(u_k, f))^2 + w(u_k, f)w(u, f) + (w(u, f))^2} \right\|_{L^2(\Omega)} \\ &\leq \left\| \frac{(\Delta u_k - \Delta u)((\Delta u_k)^2 + \Delta u_k \cdot \Delta u + (\Delta u)^2)}{(w(u_k, f))^2 + w(u_k, f)w(u, f) + (w(u, f))^2} \right\|_{L^2(\Omega)} \\ &\leq \left\| \frac{(\Delta u_k)^2 + \Delta u_k \cdot \Delta u + (\Delta u)^2}{(w(u_k, f))^2 + w(u_k, f)w(u, f) + (w(u, f))^2} \right\|_{L^\infty(\Omega)} \|\Delta u_k - \Delta u\|_{L^2(\Omega)}. \end{aligned}$$

Let $M = (M_{ij}), N = (N_{ij})$ be matrix fields and c be a real number. Then we get

$$\begin{aligned} \frac{M : N}{c} &= \frac{1}{c} \sum_{i,j=1}^3 M_{ij} N_{ij} = \sum_{i,j=1}^3 \frac{M_{ij}}{c} N_{ij} \\ &\leq \left\| \frac{M}{c} \right\|_{\infty} \sum_{i,j=1}^3 |N_{ij}| \leq \left\| \frac{M}{c} \right\|_{\infty} \left(\sum_{i,j=1}^3 N_{ij}^2 \right)^{1/2} \cdot 3, \end{aligned} \quad (27)$$

where $\left\| \frac{M}{c} \right\|_{\infty} = \max_{1 \leq i \leq 3} \sum_{j=1}^3 \left| \frac{M_{ij}}{c} \right|$. By (27) with , we have

$$\begin{aligned} &\left\| \frac{27(\det(D^2 u) - \det(D^2 u_k))}{(w(u_k, f))^2 + w(u_k, f)w(u, f) + (w(u, f))^2} \right\|_{L^2(\Omega)} \\ &\leq 27 \left\| \frac{(\text{cof}((1-t)D^2 u_k + tD^2 u) : (D^2 u_k - D^2 u))}{(w(u_k, f))^2 + w(u_k, f)w(u, f) + (w(u, f))^2} \right\|_{L^2(\Omega)} \\ &= 27 \left[\int \left(\frac{(\text{cof}((1-t)D^2 u_k + tD^2 u) : (D^2 u_k - D^2 u))^2}{(w(u_k, f))^2 + w(u_k, f)w(u, f) + (w(u, f))^2} \right)^{\frac{1}{2}} \right] \\ &= 81 \left\| \frac{\text{cof}((1-t)D^2 u_k + tD^2 u)}{(w(u_k, f))^2 + w(u_k, f)w(u, f) + (w(u, f))^2} \right\|_{\infty} \|u_k - u\|_{H^2(\Omega)} \\ &\leq 81 \left\| \frac{(1-t)D^2 u_k + tD^2 u}{(w(u_k, f))^2 + w(u_k, f)w(u, f) + (w(u, f))^2} \right\|_{\infty}^2 \|u_k - u\|_{H^2(\Omega)} \\ &\leq 81 \left\| \frac{(1-t)D^2 u_k + tD^2 u}{(w(u_k, f))^2 + w(u_k, f)w(u, f) + (w(u, f))^2} \right\|_{\infty}^2 \|u_k - u\|_{H^2(\Omega)} \end{aligned}$$

for some $t \in [0, 1]$. By these two equations, we can have

$$\begin{aligned} \|\Delta u_{k+1} - \Delta u\|_{L^2(\Omega)} &= \left\| \frac{(\Delta u_k)^3 - (\Delta u)^3 + 27(\det(D^2 u) - \det(D^2 u_k))}{(w(u_k, f))^2 + w(u_k, f)w(u, f) + (w(u, f))^2} \right\|_{L^2(\Omega)} \\ &\leq \left\| \frac{(\Delta u_k - \Delta u)((\Delta u_k)^2 + \Delta u_k \cdot \Delta u + (\Delta u)^2)}{(w(u_k, f))^2 + w(u_k, f)w(u, f) + (w(u, f))^2} \right\|_{L^2(\Omega)} \\ &\quad + \left\| \frac{27(\det(D^2 u) - \det(D^2 u_k))}{(w(u_k, f))^2 + w(u_k, f)w(u, f) + (w(u, f))^2} \right\|_{L^2(\Omega)} \\ &\leq \left\| \frac{(\Delta u_k)^2 + \Delta u_k \cdot \Delta u + (\Delta u)^2}{(w(u_k, f))^2 + w(u_k, f)w(u, f) + (w(u, f))^2} \right\|_{L^{\infty}(\Omega)} \|\Delta u_k - \Delta u\|_{L^2(\Omega)} \\ &\quad + 81 \left\| \frac{(1-t)D^2 u_k + tD^2 u}{(w(u_k, f))^2 + w(u_k, f)w(u, f) + (w(u, f))^2} \right\|_{\infty}^2 \|u_k - u\|_{H^2(\Omega)} \end{aligned}$$

for some $t \in [0, 1]$. Now, we need the following lemma from [39] to prove one of the main convergence results in this paper.

Lemma 5 Suppose that Ω is bounded and has uniformly positive reach $r_{\Omega} > 0$. Then there exist two positive constants A and B such that

$$A\|u\|_{H^2(\Omega)} \leq \|\Delta u\|_{L^2(\Omega)} \leq B\|u\|_{H^2(\Omega)}, \quad \forall u \in H^2(\Omega) \cap H_0^1(\Omega). \quad (28)$$

By Lemma 5, we have

$$\begin{aligned} \|\Delta u_{k+1} - \Delta u\|_{L^2(\Omega)} &\leq \left\| \frac{(\Delta u_k)^2 + \Delta u_k \cdot \Delta u + (\Delta u)^2}{(w(u_k, f))^2 + w(u_k, f)w(u, f) + (w(u, f))^2} \right\|_{L^\infty(\Omega)} \|\Delta u_k - \Delta u\|_{L^2(\Omega)} \\ &\quad + 81 \left\| \frac{(1-t)D^2 u_k + tD^2 u}{(w(u_k, f))^2 + w(u_k, f)w(u, f) + (w(u, f))^2} \right\|_{L^\infty(\Omega)}^2 \frac{1}{A} \|\Delta u_k - \Delta u\|_{L^2(\Omega)} \end{aligned}$$

and therefore

$$\|\Delta u_{k+1} - \Delta u\|_{L^2(\Omega)} \leq \rho_k \|\Delta u_k - \Delta u\|_{L^2(\Omega)},$$

where

$$\begin{aligned} \rho_k := & \left\| \frac{(\Delta u_k)^2 + \Delta u_k \cdot \Delta u + (\Delta u)^2}{(w(u_k, f))^2 + w(u_k, f)w(u, f) + (w(u, f))^2} \right\|_{L^\infty(\Omega)} + \\ & \frac{81}{A} \left\| \frac{(1-t)D^2 u_k + tD^2 u}{(w(u_k, f))^2 + w(u_k, f)w(u, f) + (w(u, f))^2} \right\|_{L^\infty(\Omega)}^2. \end{aligned} \quad (29)$$

We are now ready to conclude the following result

Theorem 10 Suppose that Ω is bounded and has uniformly positive reach. If $\rho_k \leq \gamma < 1$ for all $k \geq 1$, then the sequence $\{u_k\}$ from Algorithm 1 converges.

Note that our numerical experiments show that for some testing function u , we have indeed $\rho_k < 1$ while there is other testing function u which gives $\rho_k > 1$. See Figures 3 and 4. Also, it is hard to estimate ρ_k from the formula (29).

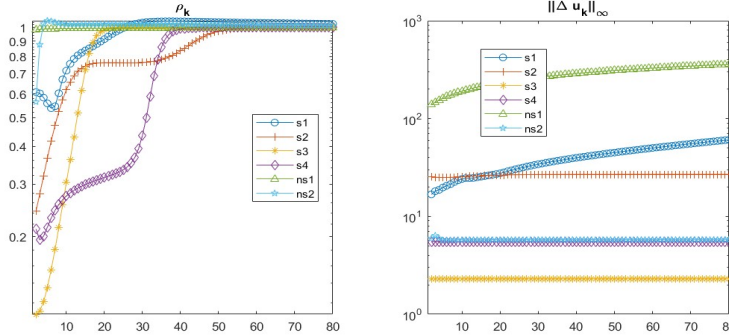


Fig. 3 ρ_k and $\|\Delta u_k\|_\infty$ for 80 iterations for smooth solutions s_1, s_2, s_3 and non-smooth solutions ns_1, ns_2

In Figures 3 and 4, we plot ρ_k corresponding to the numerical solution for smooth solutions s_1, s_2, s_3, s_4 and non-smooth solutions ns_1, ns_2 . They are defined as follows.

- s_1 : polynomial function $(x^2 + 5y^2 + 15z^2)/2$;
- s_2 : exponential function $\exp((x^2 + y^2 + z^2)/2)$;
- s_3 : radical function $-\sqrt{6 - (x^2 + y^2 + z^2)}$;
- s_4 : $(x^2 + y^2 + z^2)/2 - \sin(x) - \sin(y) - \sin(z)$;

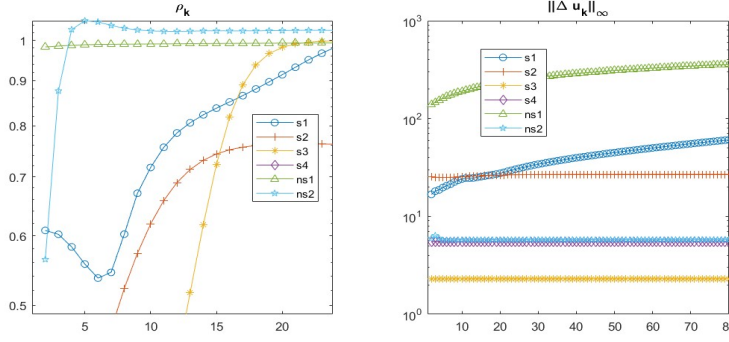


Fig. 4 An enlarged graphs in Figure 3

- $ns_1: -\sqrt{3 - (x^2 + y^2 + z^2)}$ where f is ∞ at $(1, 1, 1)$;
- $ns_2: \frac{(x^2 + y^2 + z^2)^{3/4}}{3}$ where f is ∞ at $(0, 0, 0)$.

The graphs in these figure above show that $\rho_k < 1$ and $\|\Delta u_k\|_\infty$ are bounded for smooth testing solutions. However, ρ_k may be bigger than 1 and $\|\Delta u_k\|_\infty$ may increase which maybe unbounded for nonsmooth testing functions.

When $\rho_k > 1$, the above analysis will not be useful to see convergence of the sequence $\{u_k\}$. The remaining case is $\rho_k \leq 1$. In this case, we need Algorithm 2. That is, we now study the convergence of our Algorithm 2. Letting $u^k, k \geq 1$ be the sequence from Algorithm 2, it is easy to see that

$$u_{k+1} - u^* = \frac{1}{2}(u_k - u^*) + \frac{1}{2}(T(u_k) - T(u^*)) \quad (30)$$

for all $k \geq 1$ since u^* is a fixed point of T . Since $\rho_k \leq 1$, we have $\|T(u_k) - T(u^*)\| \leq \|u_k - u^*\|$ and hence, $\|u_{k+1} - u^*\| \leq \|u_k - u^*\|$ for all $k \geq 1$. It follows that $u_k, k \geq 1$ are bounded in a $H^2(\Omega)$ norm. We now show the averaged iterative algorithm converges.

Theorem 11 Suppose that Ω is a bounded domain which has a uniformly positive reach. Suppose that $g \in H^{1/2}(\partial\Omega)$. Suppose that $\rho_k \leq 1$. Then Averaged Iterative Algorithm 2 converges.

Proof Let $S = H^2(\Omega)$. By the assumptions, the operator T defined above from S to S is a continuous and nonexpansive operator. We first recall the following equality: For any $x, y, z \in S$ and a real number $\lambda \in [0, 1]$, we have the following identity

$$\lambda\|x - z\|^2 + (1 - \lambda)\|y - z\|^2 - \lambda(1 - \lambda)\|x - z\|^2 = \|\lambda x + (1 - \lambda)y - z\|^2.$$

The proof is left to the interested reader. Let $\lambda = 1/2$ and $x = u^k, y = T(u^k)$, and $z = u^*$ which is a fixed point or the solution. Then we have

$$\begin{aligned}\|u_{k+1} - u^*\|^2 &= \frac{1}{2}\|u_k - u^*\|^2 + \frac{1}{2}\|T(u_k) - u^*\|^2 - \frac{1}{4}\|u_k - T(u_k)\|^2 \\ &= \frac{1}{2}\|u_k - u^*\|^2 + \frac{1}{2}\|T(u_k) - T(u^*)\|^2 - \frac{1}{4}\|u_k - T(u_k)\|^2 \\ &\leq \|u_k - u^*\|^2 - \frac{1}{4}\|u_k - T(u_k)\|^2.\end{aligned}$$

It follows that

$$\sum_{k=1}^N \frac{1}{4}\|u_k - T(u^k)\|^2 + \|u_{N+1} - u^*\|^2 \leq \|u^0 - u^*\|^2$$

for any integer $N > 1$. That is, $\|u_k - T(u_k)\| \rightarrow 0$ when $k \rightarrow \infty$.

We now claim that the sequence $u_k, k \geq 1$ converges. Note that due to the nonexpansiveness, $\|u_k\|, k \geq 1$ are bounded as explained above. Let \hat{u} be the limit of a subsequence of $u^k, k \geq 1$. Then we have $\hat{u} = T(\hat{u})$ by the continuity of the operator T . So \hat{u} is a fixed point of T . By the definition of T , we have

$$\Delta \hat{u} = \sqrt[3]{(\Delta \hat{u})^3 + 27(f - \det(D^2 \hat{u}))}$$

or $(\Delta \hat{u})^3 = (\Delta \hat{u})^3 + 27(f - \det(D^2 \hat{u}))$. It follows that $f = \det(D^2 \hat{u})$. Since the Monge-Ampère equation has a unique solution, we have $\hat{u} = u^*$. If there exists another \tilde{u} which is the limit of another subsequence of $u^k, k \geq 1$, we also have $\tilde{u} = T(\tilde{u})$. Then $\tilde{u} = u^*$. Hence, the sequence $\{u_k, k \geq 1\}$ from Algorithm 2 converges. \square

4 Numerical Results for 3D Monge-Ampère Equations

In this section, we present numerical results from various computational experiments. We will first test several smooth and nonsmooth solutions over convex domains, such as $[0, 1]^3$. Next, we show the numerical results over non-convex domains such as C, L, S -shaped domains. For all the experiments, we use 8 processors on a parallel computer, which has AMD Ryzen 7 4800H with Radeon Graphics 2.90 GHz. All the cases, the errors are computed based on $NI = 351 \times 351 \times 351$ equally spaced points $\{(\eta_i)\}_{i=1}^{NI}$ fell inside the domain of computation. The errors will be calculated according to the norms

$$\begin{cases} |u|_{l_2} &= \sqrt{\frac{\sum_{i=1}^{NI} (u(i))^2}{NI}} \\ |u|_{h_1} &= \sqrt{\frac{\sum_{i=1}^{NI} (u(i))^2 + (u_x(i))^2 + (u_y(i))^2 + (u_z(i))^2}{NI}} \\ |u|_{l_\infty} &= \max |u(i)|, \end{cases}$$

where $u(i) := u(\eta_i)$, $u_x(i) := u_x(\eta_i)$, $u_y(i) := u_y(\eta_i)$ and $u_z(i) := u_z(\eta_i)$ for given functions u, u_x, u_y, u_z . Tables in this section are the numerical results of $|e_s|_{l_2}$ and $|e_s|_{h_1}$, where $e_s := u - u_s$.

4.1 Smooth Testing Functions

Example 1 (Polynomial Examples) In [17], the researchers experimented the following two smooth exact solutions:

- $f^{3d1} = 75$ such that an exact solution is $u^{3ds1} = \frac{1}{2}(x^2 + 5y^2 + 15z^2)$
- $f^{3d2} = 1000$ such that an exact solution is $u^{3ds2} = \frac{1}{2}(x^2 + 10y^2 + 100z^2)$

Numerical results of their least squares/relaxation method (called LR method in this paper) are shown in Table 2. Together we present numerical results based on our spline collocation method by Algorithms 2. Table 2 shows our spline collocation

Table 2 Errors of numerical solutions u^{3ds1}, u^{3ds2} for Monge Ampère equation over $[0, 1]^3$ for LL methods with $D = 5, r = 1$ and LR method in [17]

h	LR method			
	u^{3ds1}		u^{3ds2}	
	$ e_s _{l_2}$	$ e_s _{h^1}$	$ e_s _{l_2}$	$ e_s _{h^1}$
0.2	7.19e-02	1.58e-00	2.74e-02	5.16e-01
0.1	1.80e-02	7.91e-01	7.52e-03	2.81e-01
0.0625	7.06e-03	4.95e-01	3.06e-03	1.83e-01
0.04	2.89e-03	3.16e-01	1.26e-03	1.20e-01
h	LL method			
	u^{3ds1}		u^{3ds2}	
	$ e_s _{l_2}$	$ e_s _{h^1}$	$ e_s _{l_2}$	$ e_s _{h^1}$
0.25	2.68e-07	1.01e-05	2.48e-04	4.63e-03

method (called LL method) produces more accurate solutions than those presented in [17]. The eigenvalues of the Hessian matrix are 1, 5, 15 and therefore $\det(D^2 u^{3ds1}) = \lambda_1 \lambda_2 \lambda_3 = 75$ and $\Delta u^{3ds1} = \lambda_1 + \lambda_2 + \lambda_3 = 21$. In Algorithm 2, we choose an initial value $\Delta u_0 = 14.55$ to approximate the exact solution u^{3ds1} . This choice of initial value leads to converging iterations since 14.55 is close to $\Delta u^{3ds1} = \sqrt[3]{27f} = \sqrt[3]{27 \cdot 75} = 12.65$. Similarly, we choose our initial value u_0 for u^{3ds2} satisfying $\Delta u_0 = 106.2$ which makes the iterations from Algorithm 2 converge. By choosing good initial value u_0 we achieve the numerical results shown in Table 2.

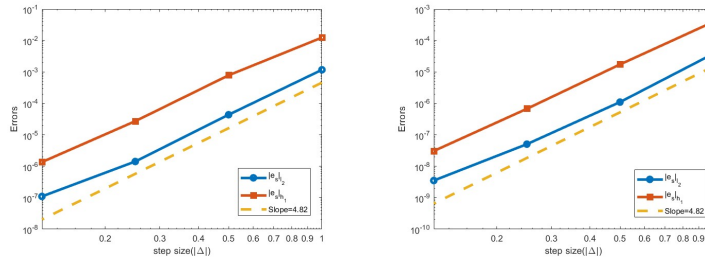
We also test other smooth solutions which were experimented in the literature, e.g., [4], [6], [17], [13], and etc..

Example 2 (Smooth Exponential Functions) Consider a smooth exponential exact solution $u^{3ds3} = e^{\frac{(x^2+y^2+z^2)}{2}}$ associated with $f^{3d3} = (1 + x^2 + y^2 + z^2)e^{\frac{3(x^2+y^2+z^2)}{2}}$. We compare our methods with the least squares/relaxation method(LR method) in [17]. Table 3 shows comparison results including l_2, h_1 norm of these two methods for each mesh size h .

We can see that better convergence results using LL methods with $D = 5, r = 1$. In Figure 5, we show plots of the $|e_s|_{l_2}, |e_s|_{h^1}$ with respect to the mesh size h . We can see that the rate of convergences is about $O(h^{4.82})$.

Table 3 Errors of numerical solutions u^{3ds3} for Monge Ampère equation over $[0, 1]^3$ for LL methods with $D = 5$, $r = 1$ and LR method in [17]

LR method					LL method				
h	$ e_s _{L_2}$	rate	$ e_s _{H^1}$	rate	h	$ e_s _{L_2}$	rate	$ e_s _{H^1}$	rate
0.2	7.19e-02	-	1.58e-00	-	1	1.17e-03	-	1.24e-02	-
0.1	1.80e-02	1.99	7.91e-01	0.99	0.5	4.36e-05	4.74	7.82e-04	3.99
0.0625	7.06e-03	1.99	4.95e-01	1.00	0.25	1.42e-06	4.94	2.72e-05	4.84
0.04	2.89e-03	1.99	3.16e-01	0.99	0.125	1.10e-07	3.69	1.36e-06	4.32

**Fig. 5** Convergence rates of l_2 , h_1 errors for solutions u^{3ds3} (Left) and u^{3ds5} (Right) with respect to $|\Delta|$ based on the LL method

Example 3 In [4] and [6], Awanou introduced the pseudo transient continuation, time marching methods and the spline element methods for Monge-Ampère equations. He presented several 2D and 3D numerical examples by his methods. For testing function $u^{3ds4} = e^{\frac{(x^2+y^2+z^2)}{3}}$, it seems that the numerical results using the spline element method (SE method) in [6] is the best. We use our spline collocation method (LL method) and compare L^2 , H^1 , H^2 errors of our method and the SE method. Table 4 and 5 show that we can get better accuracy when $h = 1$ and $h = 1/2$ for each degree $D = 4, 5, 6$.

Table 4 Errors of numerical solutions u^{3ds4} for Monge Ampère equation over $[0, 1]^3$ for LL methods with $D = 3, 4, 5, 6$, $r = 1$, $h = 1$ and SE method in [6]

D	SE method			LL method		
	L^2 norm	H^1 norm	H^2 norm	L^2 norm	H^1 norm	H^2 norm
3	1.2338e-02	7.6984e-02	4.4411e-01	1.6916e-02	1.0879e-01	3.8250e-01
4	1.6289e-03	1.4719e-02	1.3983e-01	6.4696e-04	6.1874e-03	3.7146e-02
5	1.5333e-03	8.7312e-03	6.0412e-02	1.7440e-04	2.2203e-03	1.7392e-02
6	1.2324e-04	9.7171e-04	1.0584e-02	4.6740e-05	6.2257e-04	3.5432e-03

4.2 Non-smooth Testing Functions

Example 4 In [17], the researchers considered the following problem which do not have exact solution with the $H^2(\Omega)$ -regularity or may have no solution at all. For

Table 5 Errors of numerical solutions u^{3ds4} for Monge Ampère equation over $[0, 1]^3$ for LL methods with $D = 3, 4, 5, 6, r = 1, h = 1/2$ and SE method in [6]

D	SE method			LL method		
	L^2 norm	H^1 norm	H^2 norm	L^2 norm	H^1 norm	H^2 norm
3	3.1739e-03	2.3005e-02	2.4496e-01	2.4294e-03	1.5806e-02	1.0139e-01
4	3.2786e-04	3.5626e-03	5.2079e-02	9.5591e-05	1.1644e-03	9.8077e-03
5	2.4027e-05	3.9210e-04	8.8868e-03	5.8750e-06	1.2214e-04	1.4292e-03
6	1.3821e-06	2.2369e-05	6.0918e-04	6.0635e-07	1.4198e-05	1.6487e-04

$R \geq \sqrt{3}$, let $u = -\sqrt{R^2 - (x^2 + y^2 + z^2)}$ be a testing function. When $R > \sqrt{3}$, this function belongs to $C^\infty(\bar{\Omega})$, while $u \in C^0(\bar{\Omega}) \cap W^{1,s}(\Omega)$, with $1 \leq s < 2$, if $R = \sqrt{3}$. More precisely, let us consider the following two solutions

$$u^{3ds5} = -\sqrt{6 - (x^2 + y^2 + z^2)} \quad \text{with} \quad f^{3d5} = 6(6 - (x^2 + y^2 + z^2))^{-\frac{5}{2}}$$

and

$$u^{3ds6} = -\sqrt{3 - (x^2 + y^2 + z^2)} \quad \text{with} \quad f^{3d6} = 3(3 - (x^2 + y^2 + z^2))^{-\frac{5}{2}}.$$

The numerical results from the least squares/relaxation method in [17] (called LR method) are shown in Table 6. In Figure 5, we can see that the rate of convergences of u^{3ds5} are about $O(h^{4.82})$. In addition, we show our spline collocation method (called LL method) in the same table for comparison.

Table 6 Errors of numerical approximation of the solution u^{3ds5} for Monge Ampère equation over $[0, 1]^3$ by the LR method and by the LL method with $D = 5, r = 1$

LR method					LL method				
$ \Delta $	$ e_s _{l_2}$	rate	$ e_s _{h^1}$	rate	$ \Delta $	$ e_s _{l_2}$	rate	$ e_s _{h^1}$	rate
0.2	4.96e-03	-	8.60e-02	-	1	3.75e-05	-	3.88e-04	-
0.1	1.28e-03	1.95	4.41e-02	0.96	0.5	1.10e-06	5.09	1.73e-05	4.49
0.0625	5.09e-04	1.96	2.78e-02	0.97	0.25	5.05e-08	4.45	6.73e-07	4.69
0.04	2.10e-04	1.97	1.79e-02	0.98	0.125	3.52e-09	3.84	3.06e-08	4.46

Table 7 Errors of numerical approximation of the solution u^{3ds6} for Monge Ampère equation over $[0, 1]^3$ by the LR method and by the LL method with $D = 5, r = 1$

LR method					LL method				
$ \Delta $	$ e_s _{l_2}$	rate	$ e_s _{h^1}$	rate	$ \Delta $	$ e_s _{l_2}$	rate	$ e_s _{h^1}$	rate
0.2	1.15e-02	-	6.60e-01	-	1	8.07e-02	-	7.02e-01	-
0.1	3.06e-03	1.91	6.31e-01	-	0.5	7.06e-03	3.52	1.63e-01	2.10
0.0625	1.24e-03	1.92	6.25e-01	-	0.25	4.78e-04	3.88	2.21e-02	2.89
0.04	5.17e-04	1.96	6.22e-01	-	0.125	3.85e-04	0.31	2.54e-02	-0.20
					0.0625	3.57e-04	0.11	1.98e-02	0.35

It is clear to see that when the solution u^{3ds5} is smooth, both methods work nicely and our collocation method is much accurate.

Next let us consider the non-smooth solution u^{3ds6} in Table 7. Table 7 shows numerical results such as l_2, h_1 errors of these two methods for various mesh sizes. Our method can get more accurate solution with $D = 5, r = 1$ with the large mesh size $|\Delta|$. However, it is clear that an adaptive method is needed to improve the approximation since the maximal error, $e_s = u - u_s$, is worst near the point $(1, 1, 1)$.

4.3 Numerical Results over Nonconvex Domains

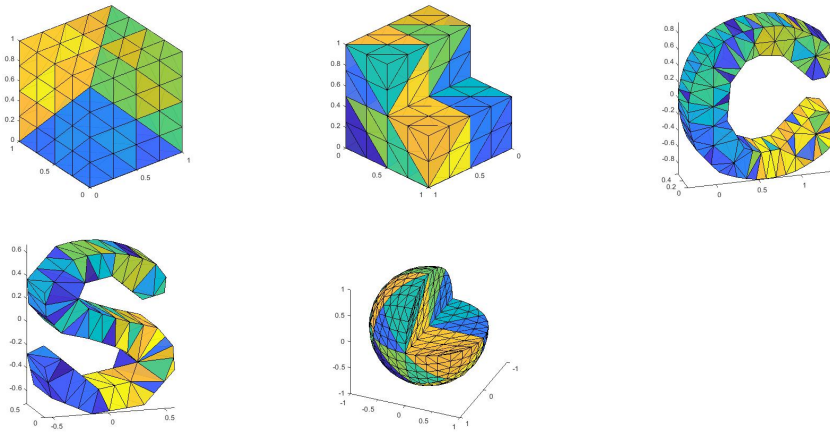


Fig. 6 Several 3D domains (Top : Cube, Letter L, Letter C , Bottom: Letter S, Subset of the unit ball)

In this section, we test various solutions for each domain in Figure 6. We display CPU times versus the number of vertices and triangles in Table 8 for each domain in Figure 6 when $D = 9, r = 1$.

Table 8 CPU time results and numbers of vertices and tetrahedrons over domains in Figure 6 when $D = 9, r = 1$

Domain	No. of Vetices	No. of Tetrahedrons	Total CPU(s)
Cube	125	384	56.0
Letter L	105	288	42.7
Letter C	190	431	129.2
Letter S	115	171	45.9

Example 5 We use our method to numerically solve three smooth testing functions $u^{3ds3}, u^{3ds4}, u^{3ds5}$ over 5 solids which are not strictly convex or not convex. They

even do not have an uniformly positive reach. Table 9 shows our method performs very well.

Table 9 Errors of numerical solutions $u^{3ds3} - u^{3ds5}$ for Monge Ampère equations over several domains in Figure 6 for LL methods with $D = 9, r = 1$

Solution	Cube		Letter L		Letter C		Letter S	
	$ e_s _{l_2}$	$ e_s _{h^1}$	$ e_s _{l_2}$	$ e_s _{h^1}$	$ e_s _{l_2}$	$ e_s _{h^1}$	$ e_s _{l_2}$	$ e_s _{h^1}$
u^{3ds3}	1.76e-09	1.64e-07	6.63e-10	2.58e-08	1.48e-08	8.67e-07	3.39e-11	1.75e-09
u^{3ds4}	2.82e-11	1.91e-10	3.90e-11	1.04e-09	2.31e-08	3.56e-07	5.84e-11	2.70e-09
u^{3ds5}	5.05e-02	3.61e-01	2.47e-08	9.56e-07	3.87e-08	3.32e-06	6.03e-10	5.03e-08

Example 6 In [17], the researchers considered the problem over the unit ball $\Omega = \{(x, y, z) | x^2 + y^2 + z^2 < 1\}$ and a convex solution

$$u^{3ds7} = -\frac{1}{2\sqrt{3}}(1 - x^2 - y^2 - z^2)$$

of the Monge-Ampère-Dirichlet problem with $f = \frac{1}{3\sqrt{3}}$. They experimented their numerical solutions (called LR method) over the unit ball as well as the 3/4 ball as shown in Figure 6.

In Table 10, we first include the numerical results from [17] and then compare the $L^2(\Omega), H^1(\Omega)$ norms of the computed approximation error $u^{3ds7} - u_s$ by our spline collocation method. In addition, we tested the solution u^{3ds7} over the subset of the

Table 10 Errors of numerical approximation of solution u^{3ds7} for Monge Ampère equation over the unit ball for the LR method and the LL method with $D = 5, r = 1$

LR method					LL method				
$ \Delta $	$ e_s _{l_2}$	rate	$ e_s _{h^1}$	rate	$ \Delta $	$ e_s _{l_2}$	rate	$ e_s _{h^1}$	rate
2.98e-01	3.26e-02	-	2.60e-01	-	1	3.71e-13	-	3.15e-12	-
1.61e-01	1.11e-02	1.74	1.28e-01	1.14	0.5	2.97e-14	3.64	1.39e-13	4.51
8.32e-02	3.22e-03	1.88	6.16e-02	1.11					
4.34e-02	9.89e-04	1.80	2.86e-02	1.17					

unit ball as shown in Figure 6. The numerical results we obtained are displayed in Table 11.

Table 11 CPU time and errors of our spline solution to u^{3ds7} for Monge Ampère equation over the domain in Figure 6 with $D = 5, r = 1$, the number of vertices=585, the number of tetrahedrons=2304

LL method		
CPU time	$ e_s _{l_2}$	$ e_s _{h^1}$
174.70	1.9005e-08	2.4941e-06

4.4 Comparison with Numerical Method in [13]

In this section, we compare our LL method with the Cascadic method in [13]. The researchers presented several examples in [13] over the irregular domains in Figure 7 by using the following test functions

$$\begin{aligned} u^{3ds3} &= e^{\frac{(x^2+y^2+z^2)}{2}}, \\ u^{3ds6} &= -\sqrt{3 - (x^2 + y^2 + z^2)}, \\ u^{3ds8} &= \frac{x^2 + y^2 + z^2}{2} - \sin(x) - \sin(y) - \sin(z), \\ u^{3ds9} &= \frac{(x^2 + y^2 + z^2)^{\frac{3}{4}}}{3}. \end{aligned}$$

We use our method (LL method) to compute numerical solutions based on the same testing functions over the same testing domains. Our numerical results are shown in Tables 12, 13 and 14.

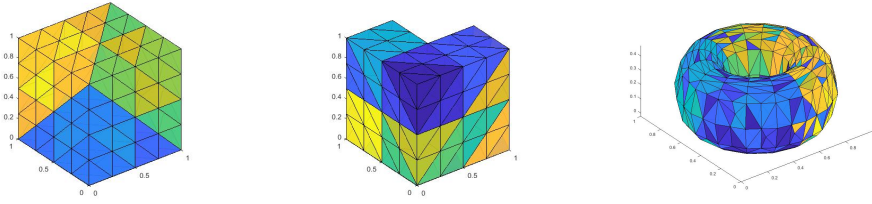


Fig. 7 Several 3D domains (Cube, Letter L, Torus)

Table 12 The CPU time, DOFs, errors $|e_s|_{l_2}$, $|e_s|_{h^1}$ using LL method with $D = 6$, $r = 1$ and $|e_s|_{l_2}$ using the Cascadic method in [13] over the cube $[0, 1]^3$

solution	LL method				Cascadic method
	CPU time	DOFs	$ e_s _{l_2}$	$ e_s _{h^1}$	$ e_s _{l_2}$
u^{3ds3}	18.712	32256	4.4010e-08	1.6144e-06	9.8659e-04
u^{3ds6}	6.9873	32256	4.0285e-04	2.6783e-02	1.7831e-04
u^{3ds8}	14.852	32256	1.8152e-11	6.8884e-10	3.5044e-04
u^{3ds9}	12.826	32256	1.3242e-04	1.1264e-03	2.2255e-04

Table 13 The CPU time, DOFs, errors $|e_s|_{l_2}$, $|e_s|_{h_1}$ using LL method with $D = 6$, $r = 1$ and $|e_s|_{l_2}$ using the Cascadic method in [13] over L-shaped domain

solution	LL method				Cascadic method
	CPU time	DOFs	$ e_s _{l_2}$	$ e_s _{h_1}$	$ e_s _{l_2}$
u^{3ds3}	12.826	24192	1.5727e-08	7.0173e-07	4.8655e-03
u^{3ds6}	4.5050	24192	6.5992e-05	7.6198e-04	1.6238e-04
u^{3ds8}	12.935	24192	1.4826e-11	6.9814e-10	1.2240e-04
u^{3ds9}	4.8951	24192	2.3076e-04	2.0929e-03	4.2183e-04

Table 14 The CPU time, DOFs, errors $|e_s|_{l_2}$, $|e_s|_{h_1}$ using LL method with $D = 4$, $r = 1$ and $|e_s|_{l_2}$ using the Cascadic method in [13] over Torus

solution	LL method				Cascadic method
	CPU time	DOFs	$ e_s _{l_2}$	$ e_s _{h_1}$	$ e_s _{l_2}$
u^{3ds3}	141.01	80990	6.0125e-07	1.3250e-05	3.1914e-04
u^{3ds6}	90.420	80990	5.6340e-04	1.1438e-02	1.9850e-04
u^{3ds8}	119.42	80990	4.9540e-07	9.5117e-06	2.1182e-04
u^{3ds9}	125.64	80990	2.3272e-07	1.3522e-05	1.7504e-04

4.5 Free Movement of Transportation

Finally, we consider the free movement problem. In this case, the Monge-Ampère equation (4) becomes

$$\det(D^2u(\mathbf{x})) = 1, \quad \mathbf{x} \text{ in } \Omega \subset \mathbb{R}^3 \quad (31)$$

$$\nabla u(\mathbf{x}) = \partial W, \quad \mathbf{x} \text{ on } \partial\Omega. \quad (32)$$

To completely determine u , we need to specify an oblique boundary condition. When both Ω and W are star-shaped domains, e.g., convex domains, we can match the centers of Ω and W by shifts and use a ray R from the center to intercept the boundary of Ω and the boundary of W . This can build up a map from $\partial\Omega$ to the boundary of W . Using the outward normal of $\partial\Omega$ and the outward normal of W , we solve the Neumann boundary condition of the Monge-Ampère equation (4) becomes

$$\det(D^2u(\mathbf{x})) = 1, \quad \mathbf{x} \text{ in } \Omega \subset \mathbb{R}^3 \quad (33)$$

$$\mathbf{n}_{\partial\Omega} \nabla u(\mathbf{x}) = \mathbf{n}_W \partial W, \quad \mathbf{x} \text{ on } \partial\Omega. \quad (34)$$

Now we can apply our computational approach to find a solution of u and form a transportation map from Ω to W . So that we can show which points in Ω is mapped to which points in W by using an image or stack of images.

Example 7 For simplicity, we first consider the 2D setting over a rectangular domain Ω and W is a circular domain as shown in Figure 8. On the left-hand side, we have an image density function and on the right-hand side, the density is transported to the circular domain. The center of the rectangular domain $\Omega = [-1, 1]^2$ is the origin $(0, 0)$ and the same for the circular domain $W = \{(x, y), x^2 + y^2 \leq 1\}$. In Figure 9

and 10, we use the point $(-0.4, 0)$ and $(0, 0.4)$ as the center of the circular domain, respectively. The image on the right-hand side of Figure 9 is clearly deformed and the similar for the image (right) of Figure 10. The cost for transportation in these two cases

$$\frac{1}{2} \int_{\Omega} \|\mathbf{x} - \nabla u(\mathbf{x})\|^2 f(\mathbf{x}) d\mathbf{x} \quad (35)$$

is larger than the cost for the transportation in Figure 8.



Fig. 8 A density over a rectangular domain $\Omega = [-1, 1]^2$ (on the left) and a transported image over the circular domain (on the right)



Fig. 9 A density over a rectangular domain $\Omega = [-1, 1]^2$ (on the left) and a transported image over the circular domain (on the right). Note the point $(-0.4, 0)$ in the circular domain was chosen as the center.

Example 8 We now show the transportation from the points in the cube $\Omega = [-1, 1]^3$ to the unit ball $W = \{(x, y, z) : x^2 + y^2 + z^2 \leq 1\}$. Again we use the density $f(\mathbf{x})$ which is a stack of the same image over Ω to show how a point in Ω is transported to the point in W .

We can see that our computation is reliable as the points in Ω are completely transported into W . In fact the map ∇u is a bijection due to the convexity of the Brenier potential u as shown in Figure 12.



Fig. 10 A density over a rectangular domain $\Omega = [-1, 1]^2$ (on the left) and a transported image over the circular domain (on the right). Note the point $(0, 0.4)$ in the circular domain was chosen as the center.

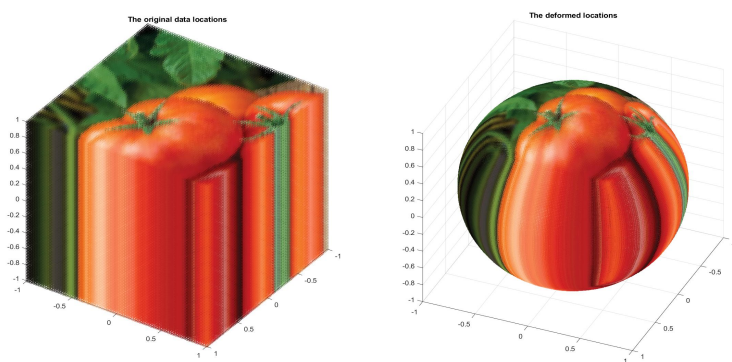


Fig. 11 A density over a rectangular domain $\Omega = [-1, 1]^3$ (on the left) and a transported image over the spherical domain W (on the right)

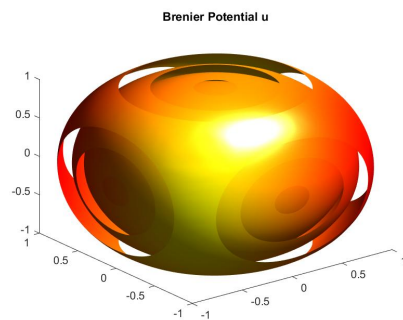


Fig. 12 An iso-surface plot of the Brenier potential over a rectangular domain $\Omega = [-1, 1]^3$

Acknowledgements The authors would like to thanks anonymous referees for their valuable comments. In addition, the authors would like to thank Dr. Gerard Awanou for generosity for providing references [22] and [55]. This work is supported by the Simons Foundation collaboration grant #864439.

References

1. S. Angenent, S. Haker, and A. Tannenbaum, Minimizing flows for the Monge-Kantorovich problem, *SIAM J. Math. Anal.*, 35, pp. 61-97 (2003)
2. Gerard Awanou, *Energy Methods in 3D Spline Approximations*, Dissertation, University of Georgia, Athens, GA, (2003)
3. Gerard Awanou, *Standard finite elements for the numerical resolution of the elliptic Monge-Ampère equation: mixed methods*, *IMA Journal of Numerical Analysis* 35(3) (2013).
4. Gerard Awanou, Pseudo time continuation and time marching methods for Monge-Ampère type equations, *Advances in Computational Mathematics* 41(4) (2013)
5. Gerard Awanou, *Standard finite elements for the numerical resolution of the elliptic Monge-Ampère equation: classical solutions*, *IMA Journal of Numerical Analysis* (2014).
6. Gerard Awanou *Spline element method for Monge-Ampère equations*, *BIT Numerical Mathematics* volume 55, pp.625-646 (2015)
7. Gerard Awanou, *On standard finite difference discretizations of the elliptic Monge-Ampère equation*, *J. Sci. Comput.* 69, 892-904 (2016).
8. Gerard Awanou, Ming-Jun Lai, and Paul Wenston, The multivariate spline method for scattered data fitting and numerical solution of partial differential equations. In *Wavelets and splines: Athens, 2005*, pages 24–74. Nashboro Press, Brentwood, TN, (2006).
9. Gerard Awanou and H. Li, *Error analysis of a mixed finite element method for the Monge-Ampère equation*, *International Journal of Numerical Analysis and Modeling* 11(4):745–761 (2014).
10. G. Barles and PE Souganidis, Convergence of approximation schemes for fully nonlinear second order equations, *Decision and Control, 1990., Proceedings of the 29th IEEE Conference on*, IEEE, pp. 2347–2349(2002)
11. J. Benamou and Y. Brenier, A computational fluid mechanics solution to the Monge- Kantorovich mass transfer problem, *Numer. Math.*, 84, pp. 375-393 (2000)
12. J.-D. Benamou, B. D. Froese and A. M. Oberman, *Two Numerical Methods for the elliptic Monge-Ampère equation*, *ESAIM: Mathematical Modelling and Numerical Analysis* (2010).
13. J.J. Benitoa, A. Garcia, L. Gavete, M. Negreanu, F. Ureña, A.M. Vargas, Solving Monge-Ampère equation in 2D and 3D by Generalized Finite Difference Method, *Engineering Analysis with Boundary Elements* 124C:52-63,(2020)
14. M. V. Berry, Oriental magic mirrors and the Laplacian image, *European J. Phys.*, 27, pp. 109-118 (2006)
15. K. Bohmer and R. Schaback, *A meshfree method for solving the Monge-Ampère equation*, *Numerical Algorithms*, vol. 82, pages 539-551(2019) .
16. K. Brix, Y. Hafizogullari and A. Platen, *Solving the Monge-Ampère equations for the inverse reflector problem*, *Mathematics, Physics* (2015).
17. Alexandre Caboussat, Roland Glowinski, Dimitrios Gourzoulidis, A Least-Squares/Relaxation Method for the Numerical Solution of the Three-Dimensional Elliptic Monge-Ampère Equation, *J. Sci. Comput.* 77:53–78 (2018).
18. L. A. Caffarelli, Interior $W^{2,p}$ estimates for solutions of the Monge-Ampère equation, *Ann. of Math.* (2) 131 (1990), 135-150.
19. L. A. Caffarelli, L. Nirenberg, J. Spruck: The Dirichlet problem for nonlinear second order elliptic equations I. Monge-Ampère equation . *Commun. Pure Appl. Math.* 37, 369–402 (1984).
20. L. A. Caffarelli and X. Cabré, Fully nonlinear elliptic equations, *American Mathematical Society Colloquium Publications*, vol. 43, American Mathematical Society, Providence, RI, (1995).
21. L.A. Caffarelli and P.E. Souganidis, A rate of convergence for monotone finite difference approximations to fully nonlinear, uniformly elliptic PDEs, *Communications on Pure and Applied Mathematics* 61, no. 1, 1–17 (2008).
22. S. Chen, J. Liu and X.-J. Wang, Global regularity for the Monge-Ampère equation with natural boundary condition, *Ann. of Math.* 194(3): 745-793(2021)

23. E. J. Dean and R. Glowinski, Numerical solution of the two-dimensional elliptic Monge-Ampère equation with Dirichlet boundary conditions: an augmented Lagrangian approach, *C. R. Math. Acad. Sci. Paris* 336 , no. 9, 779–784 (2003)
24. E. J. Dean and R. Glowinski, Numerical solution of the two-dimensional elliptic Monge-Ampère equation with Dirichlet boundary conditions: a least-squares approach, *C. R. Math. Acad. Sci. Paris* 339 , no. 12, 887–892 (2004)
25. L.C. Evans, Partial differential equations and Monge-Kantorovich mass transfer, *Lecture Notes* (1998)
26. X. Feng, Convergence of the vanishing moment method for the Monge-Ampère equation, *Trans. Am. Math. Soc.* (2008, submitted).
27. X. Feng and M. Neilan, Mixed finite element methods for the fully nonlinear Monge-Ampère equation based on the vanishing moment method, *SIAM J. Numer. Anal.* 47 , no. 2, 1226–1250 (2009)
28. A. Figalli, *The Monge-Ampère Equation and Its Applications*, European Mathematical Society (2017)
29. B. Froese and A. Oberman, Convergent finite difference solvers for viscosity solutions of the elliptic Monge-Ampère equation in dimensions two and higher, *SIAM J. Numer. Anal.*, 49 , pp. 1692–1714 (2011)
30. B. D. Froese, A Numerical Method for the Elliptic Monge-Ampère Equation with Transport Boundary Condition, *SIAM J. Sci. Comput.*, 34(3), A1432–A1459. (28 pages) (2012)
31. F. Gao and M. -J. Lai, A new H^2 regularity condition of the solution to Dirichlet problem of the Poisson equation and its applications, *Acta Mathematica Sinica*, vol. 36 pp. 21–39 (2020)
32. D. Gilbarg and N. S. Trudinger, Elliptic partial differential equations of second order, vol. 224 of *Grundlehren der Mathematischen Wissenschaften*, Springer, Heidelberg, 2nd ed., (1983).
33. D. Gilbarg and N. S. Trudinger, *Elliptic Partial Differential Equations of Second Order*. Reprint of the 1998 Edition, *Classics in Mathematics*, Springer, (2001)
34. E. Haber, T. Rehman, and A. Tannenbaum, An efficient numerical method for the solution of the L_2 optimal mass transfer problem, *SIAM J. Sci. Comput.*, 32 , pp. 197–211 (2010)
35. H.J. Kuo and N.S. Trudinger, Discrete methods for fully nonlinear elliptic equations, *SIAM Journal on Numerical Analysis* 29 , no. 1, 123–135 (1992)
36. H.J. Kuo and N.S. Trudinger, On the discrete maximum principle for parabolic difference operators, *Modélisation mathématique et analyse numérique* 27 , no. 6, 719–737 (1993)
37. H.J. Kuo and N.S. Trudinger, Positive difference operators on general meshes, *Duke Mathematical Journal* 83 , no. 2, 415–434 (1996)
38. H.J. Kuo and N.S. Trudinger, Evolving monotone difference operators on general space-time meshes, *Duke Mathematical Journal* 91 , no. 3, 587–608 (1998)
39. M.J. Lai and J. Lee, A Multivariate Spline based Collocation Method for Numerical Solution of PDEs, *SIAM J. Numerical Analysis*, vol. 60 (2022) pp. 2405–2434
40. M.-J. Lai and L. L. Schumaker, *Spline function on triangulations*, Cambridge University Press, (2007)
41. M. -J. Lai and Wenston, P., Bivariate Splines for Fluid Flows, *Computers and Fluids*, vol. 33 pp. 1047–1073 (2004)
42. J. Lee, A Multivariate Spline Method for Numerical Solution of Partial Differential Equations, Dissertation (under preparation), University of Georgia, (2023).
43. N. Lei and X. Gu, FFT-OT: A Fast Algorithm for Optimal Transportation, *ICCV* (2021)
44. J. Liu, B. D. Froese, A. M. Oberman and M. Xiao, *A multigrid scheme for 3D Monge-Ampère equations*, *International Journal of Computer Mathematics*, (2016)
45. Z. Liu and Q. Xu, *On Multiscale RBF Collocation Methods for Solving the Monge-Ampère Equation*, *Mathematical Problems in Engineering* Volume, Article ID 1748037, 10 pages (2020)
46. S.-Y. Mak and D.-Y. Yip, Secrets of the chinese magic mirror replica, *Phys. Ed.*, 36, pp. 102–107 (2001)
47. C. Mersmann, Numerical Solution of Helmholtz equation and Maxwell equations, Ph.D. Dissertation, University of Georgia, Athens, GA (2019)
48. A.M. Oberman, Wide stencil finite difference schemes for the elliptic Monge-Ampère equation and functions of the eigenvalues of the Hessian, *Discrete Contin. Dyn. Syst. Ser. B* 10 , no. 1, 221–238 (2008)
49. A.M. Ostrowski, *Solution of Equations and Systems of Equations*, Pure and Applied Mathematics, vol. IX. New York-London: Academic Press, pp. ix +202 (1960)
50. V. I. Oliker and L. D. Prussner, On the numerical solution of the equation $\frac{\partial^2}{\partial x^2} u \frac{\partial^2}{\partial y^2} u - \left(\frac{\partial^2}{\partial x \partial y} u \right) = f$ and its discretizations, I, *Numerische Mathematik* 54 , no. 3, 271–293 (1989)
51. L. L. Schumaker, *Spline Functions: Computational Methods*. SIAM Publication, Philadelphia (2015).
52. L. L. Schumaker, Solving elliptic PDE's on domains with curved boundaries with an immersed penalized boundary method. *J. Sci. Comput.* 80 , no. 3, 1369–1394 (2019)
53. C. Villani, *Topics in Optimal Transportation*, AMS, Providence, RI, (2003).

-
54. C. Villani, Optimal transport: old and new, volume 338. Springer Science & Business Media, (2008).
 55. X.-J. Wang, Regularity for Monge-Ampère equation near the boundary, *Analysis* 16 (1996), 101-107
 56. Y. D. Xu, Multivariate Splines for Scattered Data Fitting, Eigenvalue Problems, and Numerical Solution to Poisson equations, Ph.D. Dissertation, University of Georgia, Athens, GA,(2019)
 57. X. Zhu, J. Ni, and Q. Chen, An optical design and simulation of LED low-beam headlamps, *J. Phys. Conf. Ser.*, 276, p. 012201(2011)